

XIN ZENG<sup>1,2</sup>, XIAOXIAO WANG<sup>1,2</sup>, XUECHENG PING<sup>1,2\*</sup>, RENJIE WANG<sup>1,2</sup>, TAO HU<sup>3</sup>

## RESEARCH ON FRETTING FATIGUE OF TUNGSTEN CARBIDE COATING BASED ON STRAIN ENERGY DENSITY METHODS

The numerical solutions of stress and strain components on the critical plane of tungsten carbide coating were solved based on the critical plane method in three-dimensional coordinate system, and accordingly three strain energy density parameters (Smith-Watson-Topper, Nita-Ogatta-Kuwabara and Chen parameters) were determined to reveal the fretting fatigue characteristics of tungsten carbide coating. In order to predict the fretting fatigue life based on the strain energy density criterion, the expressions between the strain energy density parameter and the fretting fatigue life was obtained experimentally. After the comparison of the three strain energy parameters, it was found that all three parameters could accurately predict the crack initiation position, but only the Smith-Watson-Topper parameters could accurately predict the crack initiation angle. The effects of cyclic load, normal load and friction coefficient on fretting fatigue damage behaviors were discussed by using the Smith-Watson-Topper criterion. The results show that the fretting fatigue life decreases with the increase of cyclic load; an increase in the normal contact load will cause the Smith-Watson-Topper damage parameters more concentrated at the outer edge of the bridge foot; a decrease in the friction coefficient will increase the Smith-Watson-Topper damage parameters in the middle of the contact surface.

*Keywords:* WC coating; crack initiation; cracking angle; critical plane; life prediction

### 1. Introduction

Coating technology has the ability to improve the wear resistance of parts surface or repair the surface of damaged parts without affecting the basic mechanical properties of matrix materials. Therefore, it is favored by aerospace, metallurgical engineering, mechanical engineering, packaging and printing, etc. Among them, Tungsten Carbide (WC) coating is widely used in aviation field instead of hard chromium electroplating as a surface strengthening method because of its mechanical, physical and chemical properties such as high hardness, high strength, high temperature resistance, wear resistance and corrosion resistance [1-3].

In order to verify the safety of WC coating over the life of component, scholars have conducted extensive research on the strength, failure mode and fatigue of WC coatings. Kubaik et al. verified the improvement effect of high-speed flame spraying Tungsten Carbide-Cobalt (WC-Co) coating and shot peening strengthening process on fretting wear through experiments, and also studied the inhibition effect on fretting fatigue crack

initiation and propagation [4]. Benea et al. compared the fretting and wear behavior of nano Tungsten Carbide-Nickel (WC-Ni) coatings in dry or wet environments, focusing on demonstrating the advantages of the coating [5]. Liu et al. [6] and Luo et al. [7] used an experimental method to obtain the fretting diagram, which accurately established the relationship between the fretting behavior and the wear degree. Lee et al. deeply studied the reasons for improving fracture toughness by heat treatment, and conducted research on the grain coarsening behavior and decarburization of WC [8]. From the above studies, it can be seen that most of them are on the fretting wear of WC coatings, which is related to the initial purpose of the coating to increase the wear resistance of the surface. Relatively speaking, there is a lack of research results in fretting fatigue. However, during the use of mechanical connecting components sprayed with WC coating, fretting fatigue damage is easy to occur between the contact surfaces, resulting in the significant reduction of the fatigue strength of connecting parts. At the same time, the service life of components becomes more uncertain, which cannot be ignored especially in the aviation industry.

<sup>1</sup> TIANJIN UNIVERSITY OF SCIENCE AND TECHNOLOGY, SCHOOL OF MECHANICAL ENGINEERING, TIANJIN 300222, CHINA

<sup>2</sup> TIANJIN UNIVERSITY OF SCIENCE AND TECHNOLOGY, TIANJIN KEY LABORATORY OF INTEGRATED DESIGN AND ONLINE MONITORING OF LIGHT INDUSTRY AND FOOD ENGINEERING MACHINERY AND EQUIPMENT, TIANJIN 300222, CHINA

<sup>3</sup> SHANGHAI XIFA BUSINESS CONSULTING CO., LTD., SHANGHAI 200232, CHINA

\* Corresponding author: xuechengping@hotmail.com



A large number of previous experiments and numerical results have demonstrated that the surface in the fretting region is in a multiaxial stress state [9]. Vázquez et al. [10] have evaluated the multiaxial fatigue parameters of Al7075-T651 alloy in predicting the location and orientation of fretting fatigue crack. Nitta et al. [11] investigated multiaxial and low cycle fatigue behavior of 304 stainless steel in high temperature environments. Chen et al. [12] established the strain energy density model for mixed-mode fracture. It can be seen from the above discussions that the methods have not been used to solve the fretting fatigue problem of WC coated parts. Therefore, it is necessary to establish a method suitable for predicting the fretting fatigue life of WC coatings and research the factors affecting the fretting fatigue.

In this paper, the fretting fatigue life of WC-12Co coatings will be predicted based on the multiaxial fatigue theory of strain energy density method. First, the damage parameters of Smith-Watson-Topper (SWT), Nita-Ogatta-Kuwabara (NOK) and Chen (CHEN) are determined according to the stress and strain components in the critical plane, and the fretting fatigue life prediction formula is established. Then, the material parameters in the fatigue life prediction formula are determined through the fretting fatigue experiment of WC-12Co coating. Finally, the effects of cyclic load, normal contact load and friction coefficient on the location and life of fretting fatigue damage are investigated. This will provide a feasible method for predicting the fretting fatigue behavior of WC coating, greatly reducing the maintenance cost of mechanical components.

## 2. Experimental details

The geometric dimensions of the specimen in this study are shown in Fig. 1 [13]. The WC-12Co powder was sprayed by high velocity oxygen-fuel (HVOF) with a coating thickness of 0.5 mm. The X-ray Diffraction (XRD) results of the coating samples are shown in Fig. 2. The composition of the coating is mainly WC phase, and there is a small amount of  $W_2C$  phase and  $Co_3W_3C$  phase formed by the oxidation of WC due to high temperature spraying. The measured chemical composition of the WC-12Co coating is shown in TABLE 1 [14].

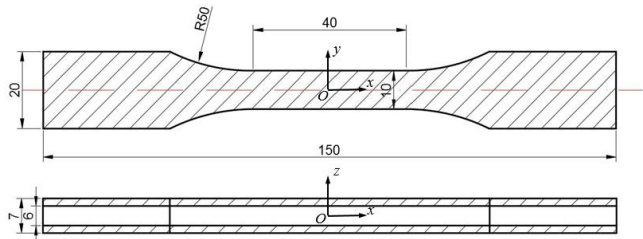


Fig. 1. Diagram of WC-Co coated specimen size

The material properties of the WC coating specimens before the experiment were measured. Firstly, the elastic modulus and Poisson's ratio of the WC coating of the experimental specimen were measured by three-point bending test [15], which are

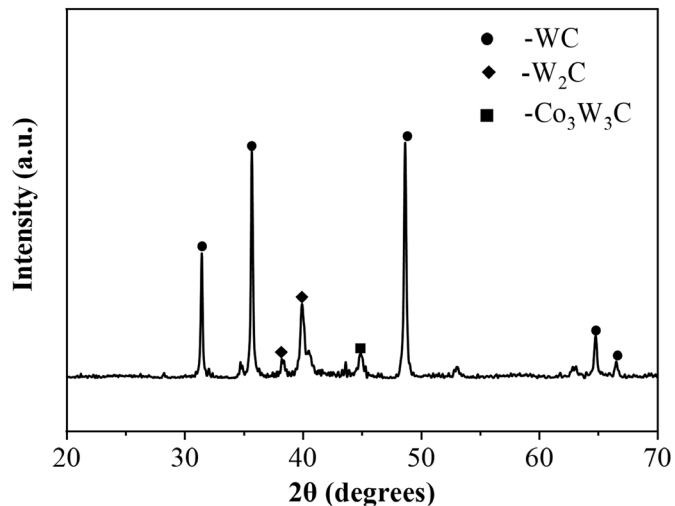


Fig. 2. XRD spectra of WC-Co coating

TABLE 1

Chemical composition of WC-12Co coating (wt.%)

Elements	C	W	Co	O	Cr	N	Fe
wt%	22.65	38.60	12.72	17.42	6.050	1.630	0.9300

319 GPa and 0.27, respectively. The surface roughness parameter measured by the surface roughness instrument (Mitutoyo, Surftest SJ-210) is  $Ra\ 2.9\ \mu m \div Ra\ 3.6\ \mu m$ . The section of the specimen after grinding and cleaning was observed by scanning electron microscope (SEM). As shown in Fig. 3(a), the coating is closely combined with the substrate, the joint is serrated, and there are few microcracks, pores and other defects at the interface. Fig. 3(b) shows the surface morphology of the tungsten carbide coating. The coating surface is not smooth, and some particles are still not melted. There are void defects due to the incomplete spreading of the particles, which may be caused by the impact of WC particles. Fig. 3(c) is the enlarged view of coating surface morphology. It shows that the cobalt phase is semi-melted or completely melted in the process of HVOF spray, which effectively inhibits the decomposition of WC particles. At the same time, cobalt acts as a connecting phase, it bonds the unmelted polygonal WC particles together.

As shown in Fig. 4(a), the tensile fretting fatigue experiment was carried out on an electro-hydraulic servo fatigue testing machine (Landmark 370.10). As shown in Fig. 4(b), the normal fretting contact load is applied through the contact pad. The contact pad is a bridge-typed pad designed according to Japanese Society of Mechanical Engineers (JSME) standard [16]. The pad is made of Gr12MoV bearing steel, which clamp the specimen from two opposite sides. Experiments were performed at room temperature, the test tensile loading frequency is fixed at 20 Hz, the stress ratio  $R$  is equal to 0, and five levels of stresses are taken from high to low for fatigue test.

The test specimen and a bridge foot form a rectangular contact area, and the normal contact pressure  $P$  on the two pads is changed by adjusting the bolt on the loading ring. The

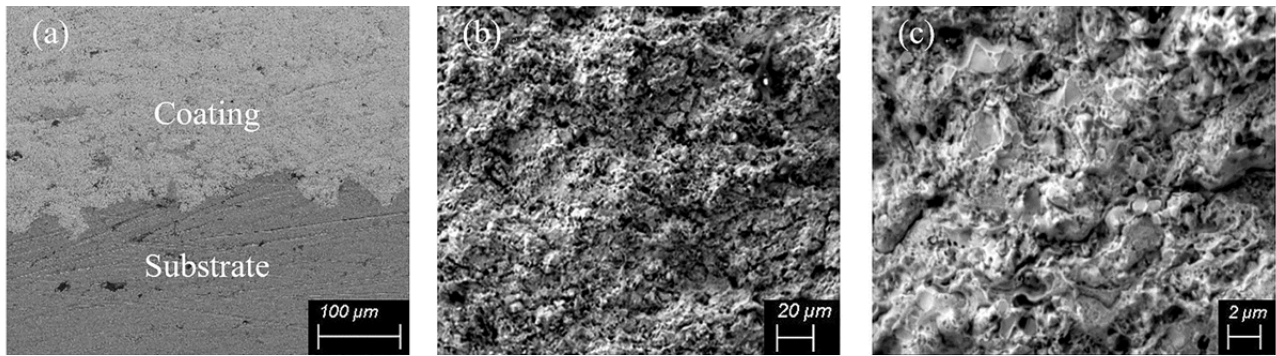


Fig. 3. Coating morphology: (a) coating-substrate interface; (b) coating surface morphology; (c) enlarged view of coating surface morphology

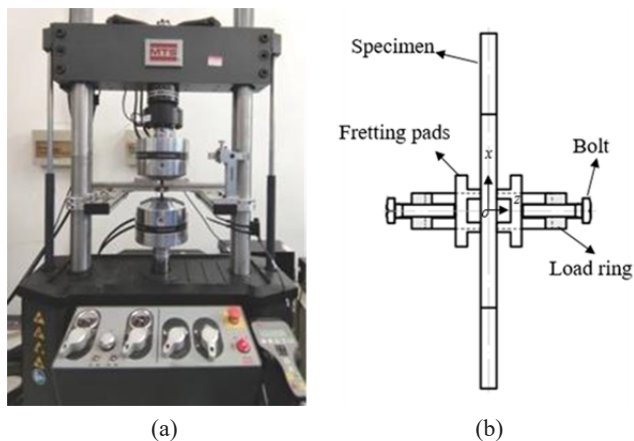


Fig. 4. Experimental setup: (a) fatigue testing machine; (b) preloading fixture

deformation of the ring is measured by the strain gauges on both sides of the loading ring, and measured by the Wheatstone bridge circuit to eliminate the deformation changes caused by temperature changes or other environmental factors. The strain of the loading ring can be used to determine the normal load  $P$ . At here, the load applied on the two pads is set as  $P = 130$  MPa.

### 3. Numerical simulation method

In this section, a fretting fatigue simulation model is established for the WC-12Co coating. Through this model, the evolution process of mating surface profile, key contact parameters and axial stress distribution with cycle count can be quantitatively simulated, thus providing a basis for the prediction of fretting fatigue crack initiation.

#### 3.1. Finite element analysis model

The three-dimensional model was established by using the commercial finite element software ABAQUS [17]. Since the shape and stress state of the WC-12Co coated specimen are symmetrical, in order to shorten the calculation time, a 1/8 model as shown in Fig. 5 was established. The basic material parameters of WC-12Co coating and 18Cr2Ni4WA substrate are listed in

TABLE 2.  $E_a$ ,  $\nu_a$  and  $\sigma_{sa}$  are the elastic modulus, Poisson's ratio and yield strength of 18Cr2Ni4WA, respectively; and  $E_b$ ,  $\nu_b$  and  $\sigma_s$  are the elastic modulus, Poisson's ratio and yield strength of the WC-12Co, respectively. Both WC-12Co coating and 18Cr2Ni4WA substrate materials are discretized by C3D8R element [17]. In the geometric model, there is stress concentration at the contact edge between the bridge foot and the specimen, and the mechanical behavior here is very complex because of the existence of normal pressure. Therefore, the mesh near the contact part is set to a minimum of 0.1 mm in order to reduce the errors of the simulation results. A contact pair is set up using a master-slave contact method, where the coating contact surface is considered as the master surface and the bridge foot surface is considered as the slave surface. The friction coefficient  $f$  between the contact surfaces is chosen to be 0.5. In the numerical simulation, the effects of cyclic loads  $F$  of 8 kN, 8.5 kN, 9 kN, 9.5 kN and 10 kN were evaluated. In the experiment, the cyclic load is applied to the free end, and the stress ratio  $R = 0$ , which means that the specimen is always in tension.

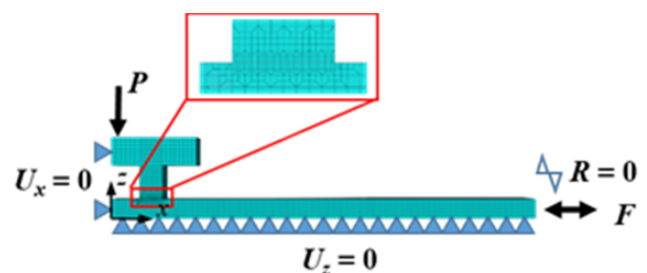


Fig. 5. Finite element model of the WC-12Co coated specimen and the contact pad for the fretting fatigue problem

TABLE 2

Basic physical parameters of materials of the WC-12Co coated specimen

Materials	Basic physical parameters
18Cr2Ni4WA	$E_a = 202$ GPa, $\nu_a = 0.273$ , $\sigma_{sa} = 1180$ MPa;
WC-12Co	$E_b = 319$ GPa, $\nu_b = 0.27$ , $\sigma_{sb} = 1300$ MPa;

Before the fatigue crack initiation analysis, the contact state along the  $x$ -axis of the contact area in the finite element model is first extracted. Fig. 6(a) shows the results of the contact pres-

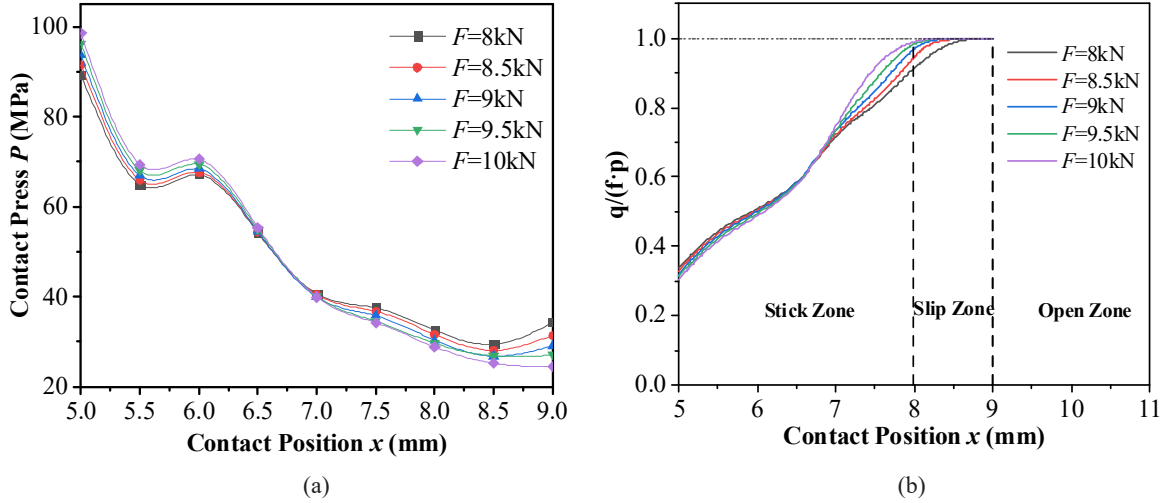


Fig. 6. (a) Contact pressure under tension load  $F$ ; (b) Contact status under tension load  $F$

sure  $P$  for the fretting fatigue specimen under the condition of  $R = 0$  and different cyclic stresses. It can be seen that since the normal contact load is applied to the center area of the fretting pad through the bolt, the contact pressure inside the contact area is much larger than that outside the contact area. Inside the contact area, the contact pressure increases with the increase of the axial cyclic load; at  $x = 6.9$ , the contact stress produced by different cyclic axial loads is the same, while the contact pressure outside the contact area decreases with the increase of axial cyclic load. As shown in Fig. 6(b), the state of the contact area is divided into adhesion area and sliding area. The adhesion area is determined by the sliding friction force  $Q(x) (=fP(x))$ , in which  $f$  is the friction coefficient and the  $P(x)$  is the contact pressure at position  $x$ . When the slip state  $Q(x) \leq fP(x)$ , the area is the adhesion area [18]. Under the premise of keeping the position and amplitude of the normal load unchanged, it is found that the percentage of adhesion area decreases with increasing of axial stress.

### 3.2. Life prediction model based on strain energy density criterion

Under the fretting condition, in addition to the external load, the fretting contact surface of the specimen is also subjected to pressure and friction. Therefore, the prediction of fretting fatigue life can be based on the multiaxial fatigue strength theory. Up to now, a variety of multiaxial fatigue damage models have been proposed. Most of these damage models adopt the critical plane method (the plane where the maximum damage parameter of the material is located in the service process is taken as the critical plane). The damage parameter based on the strain energy density is a more accurate prediction method compared with those based on strain or stress, and easy to explain the initiation mechanism of fatigue cracks. The strain energy density damage parameter  $\Delta W$  is defined as the product of the stress and strain components [10-12]:

$$\Delta W = \alpha \Delta \sigma \Delta \varepsilon + \beta \Delta \tau \Delta \gamma \quad (1)$$

where  $\alpha$  and  $\beta$  are coefficients;  $\Delta \sigma$ ,  $\Delta \varepsilon$ ,  $\Delta \tau$  and  $\Delta \gamma$  are the stress, strain, shear stress and shear strain increment on the critical plane, respectively;  $\alpha \Delta \sigma \Delta \varepsilon$  term represents the tensile force component;  $\beta \Delta \tau \Delta \gamma$  term represents the shear force component. The critical plane method finally finds the plane with the largest damage parameter by comparing the damage parameters of all plane orientations at a point on the contact surface. After the stress-strain data of each load increment step are obtained through finite element analysis, the transformation of shear stress and normal stress in any direction can be solved by Mohr circle [10-12]:

$$\sigma_{x'} = \frac{\sigma_x + \sigma_y}{2} + \frac{\sigma_x - \sigma_y}{2} \cos(2\theta) + \tau_{xy} \sin(2\theta) \quad (2)$$

$$\sigma_{y'} = \frac{\sigma_x + \sigma_y}{2} - \frac{\sigma_x - \sigma_y}{2} \cos(2\theta) - \tau_{xy} \sin(2\theta) \quad (3)$$

$$\tau_{x'y'} = \frac{\sigma_x - \sigma_y}{2} \sin(2\theta) + \tau_{xy} \cos(2\theta) \quad (4)$$

where  $\sigma_{x'}$ ,  $\sigma_{y'}$  and  $\tau_{x'y'}$  are the stress components on the critical plane,  $\sigma_x$ ,  $\sigma_y$  and  $\tau_{xy}$  are the stress components in the principal coordinates, and  $\theta$  is the critical plane.

Let the angle increment  $\Delta \theta = 1^\circ$  and  $0^\circ \leq \theta \leq 180^\circ$ , then all nodes on the contact surface have 180 different sections under each load step. The direction of the critical plane can be judged according to the stress and strain on each section. In the present work, three fretting fatigue parameters of SWT, NOK and CHEN on the critical plane are solved respectively.

Smith et al. comprehensively considered the effects of uniaxial stress and strain under the action of tensile loading, and proposed a SWT damage parameter [10]:

$$\text{SWT} = \sigma_{\max} \frac{\Delta \varepsilon}{2} = \frac{(\sigma'_f)^2}{E} (2N_f)^{2b} + \sigma'_f \varepsilon'_f (2N_f)^{b+c} \quad (5)$$

where  $E$  is the elastic modulus of the material,  $\sigma'_f$  is the fatigue strength coefficient,  $b$  is the fatigue strength exponent,  $\varepsilon'_f$  is the fatigue toughness coefficient, and  $c$  is the fatigue toughness exponent.

NOK criterion is a strain energy density criterion based on crack mode and load type. For the crack problem under proportional load, the normal strain energy density is used as the fatigue damage parameter, the product of the maximum normal stress amplitude  $\Delta\sigma/2$  and the maximum normal strain range  $\Delta\varepsilon_1$  is used as a damage parameter to calculate the fatigue life [11]:

$$\text{NOK} = \frac{\Delta\sigma_1}{2} \Delta\varepsilon_1 = A_1 N_f^{-\beta_1} \quad (6)$$

where  $A_1$  and  $\beta_1$  are both material constants.

Chen et al. proposed a multiaxial fatigue damage parameter and successfully introduced the parameters based on shear stress to predict the fretting fatigue initiation life, location and direction. The model is defined as follows [12]:

$$\begin{aligned} \text{CHEN} &= \Delta\sigma_1 \Delta\varepsilon_1 + \Delta\tau_1 \Delta\gamma_1 = \\ &= \frac{\sigma'_f}{E} (2N_f)^{2b} + 4\sigma'_f \varepsilon'_f (2N_f)^{b+c} \end{aligned} \quad (7)$$

The above three models are all based on typical energy density damage parameters. In order to apply these models,

the undetermined coefficients must be calibrated in advance. If the maximum values of the fatigue damage parameters of the specimen under different cyclic loads are calculated, the undetermined material parameters in the three models can be calculated combined with the actual fretting fatigue life obtained from the experiment. According to the experimental results, the material parameters on the right side of the Eq. (5)-Eq. (7) are listed in TABLE 3, they are determined from the fitted curve as shown in Fig. 7. With given damage parameters, the predicted fretting fatigue life and experimental fretting fatigue life of the WC-12Co coated specimen are shown in Fig. 8. It can be seen that the predicted life is consistent with the experimental life, and the error is less than 2 times of the error factor.

TABLE 3

Material parameters for the three models	
Failure criterion	Material parameters
SWT	$\sigma'_f = 581.2, b = -0.1391, \varepsilon'_f = 1.300 \cdot 10^{-7}, c = -4.291$
NOK	$A_1 = 1.111, \beta_1 = 0.1173$
CHEN	$\sigma'_f = 421.0, b = -0.1391, \varepsilon'_f = 1.300 \cdot 10^{-7}, c = -1.717$

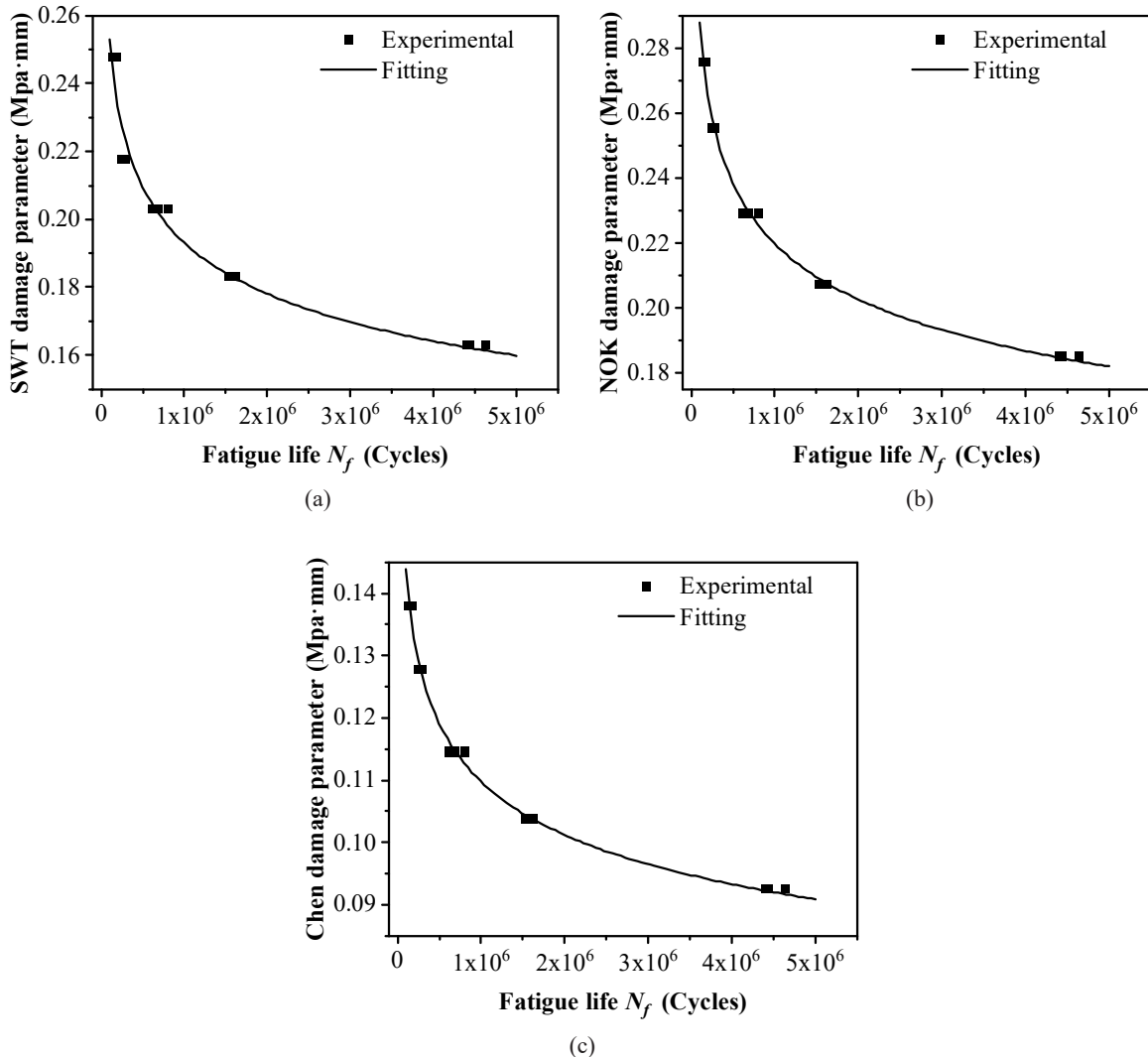


Fig. 7. Relationships between damage parameters and experimental lives of WC coated specimens. (a) SWT versus  $N_f$  curve, (b) NOK versus  $N_f$  and (c) CHEN versus  $N_f$

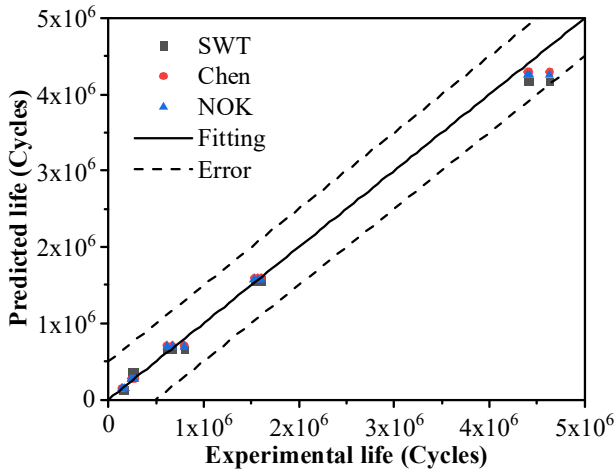


Fig. 8. Predicted and experimental life of WC coated specimens

#### 4. Results and discussion

In this section, the fretting fatigue experiment of WC-12Co coating is discussed, the location and angle of fretting fatigue

crack initiation are predicted, and the influence of related influencing factors on fretting fatigue behavior is discussed. The conclusions are drawn by comparing the experimental results with the predicted results of the model.

##### 4.1. Prediction of fretting fatigue crack initiation location and orientation

The location of the maximum fatigue damage parameter is the crack initiation location, and the direction of the critical plane where the maximum fatigue damage parameter located is the direction of crack initiation. Fig. 9 shows the profile of the fretting fatigue crack initiation location predicted by the three models. Fig. 9 are the contours of fretting fatigue damage parameters when the cyclic load is 8 kN, 9 kN and 10 kN, respectively. It can be seen that for the prediction of crack initiation location, the results given by NOK model and CHEN model are basically consistent, the predicted crack initiation position is relatively closer to the contact edge than the SWT model. When the cyclic axial load  $F = 9$  kN, the fatigue damage parameters of the

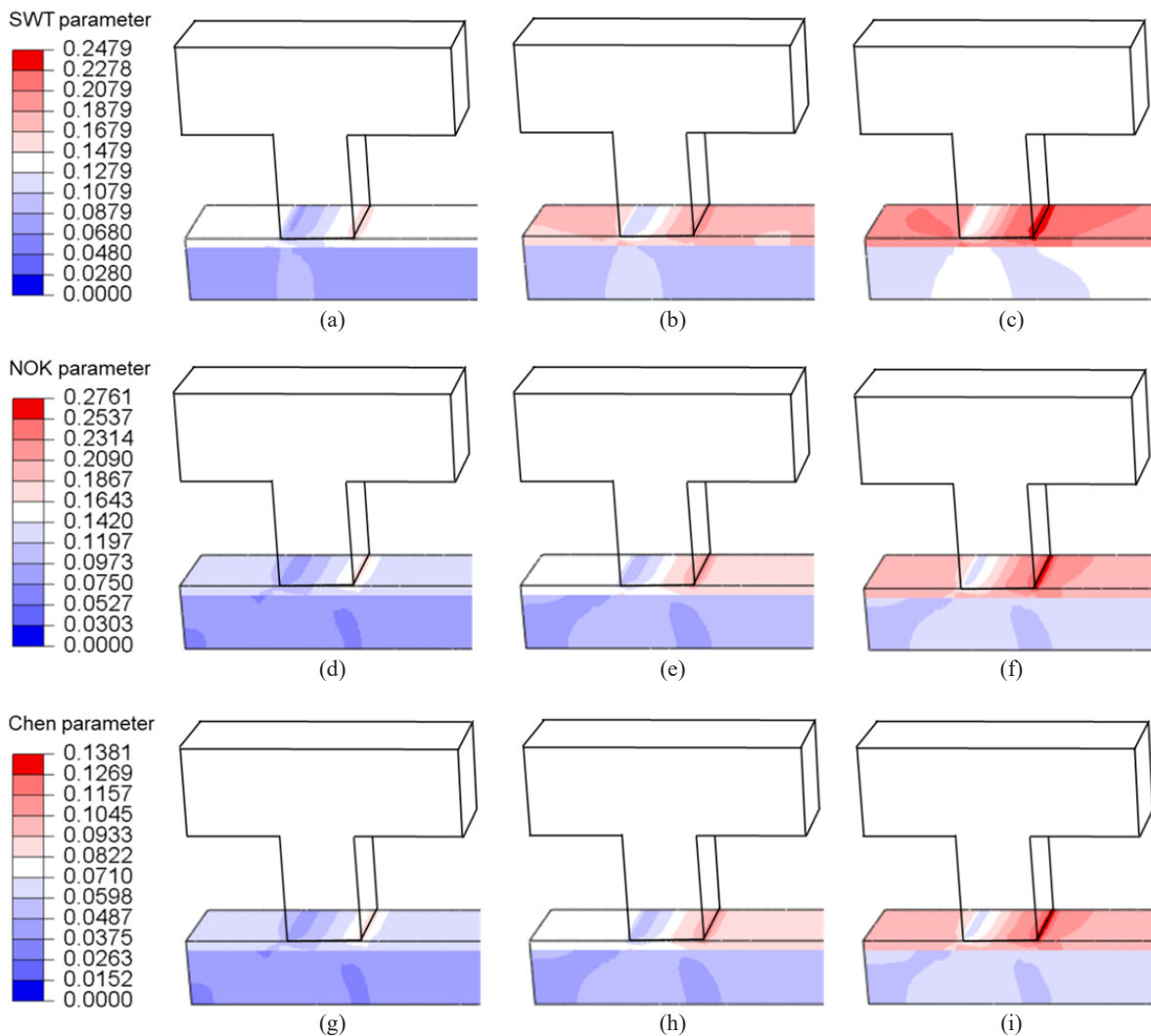


Fig. 9. Contour of the fretting fatigue parameters under cyclic loading  $F$  of 8 kN (a, d, g), 9 kN (b, e, h) and 10 kN (c, f, i) by SWT model (a, b, c), NOK model (d, e, f) and CHEN model (g, h, i)

three models along the  $x$ -axis in the contact area are shown in Fig. 10. At  $x = 5.25$  mm, the three fatigue damage parameters all have a minimum value. Then they increase with increasing of  $x$ -coordinate, and all reach the maximum value at  $x = 9$  mm.

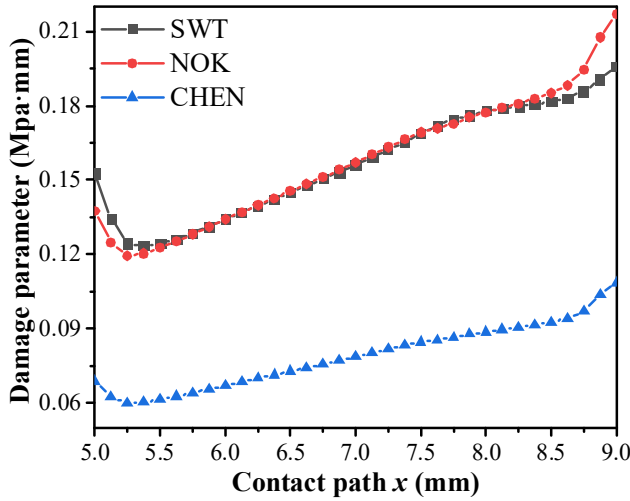


Fig. 10. Different damage parameters of WC-12Co coated specimens along contact path

Although the three models predicted different fatigue damage parameters, the trends along the  $x$ -axis in the contact area were roughly the same, so it does not affect the judgment of fretting fatigue crack initiation location.

When other conditions remain unchanged, only changing the amplitude of the axial cyclic load  $F$ , all three fretting fatigue parameters predict the location of crack initiation near the outer edge of the contact pad ( $x = 9$  mm,  $z = 3.5$  mm), and when the axial cyclic load is increased, the crack initiation location is closer to the contact edge. As shown in Fig. 11(a), it can be seen that obvious wear traces are produced at the initial stage of crack initiation, and they are basically concentrated at the outer edge of the contact area between the fretting pad and the specimen ( $x = 9$  mm). Fig. 11(b) is the picture of the specimen after fracture in fretting fatigue test, and the fracture position also appears at the outer edge of the contact surface between fretting pad and the specimen. The experimental results are the same as the predicted locations of the three fretting fatigue parameters, and cracks are likely to be initiated near the outer edge of the contact area between the bridge foot and the specimen, where the bridge foot and the specimen are severely worn. Fig. 11(c) is the fracture morphology at the fracture location. According to

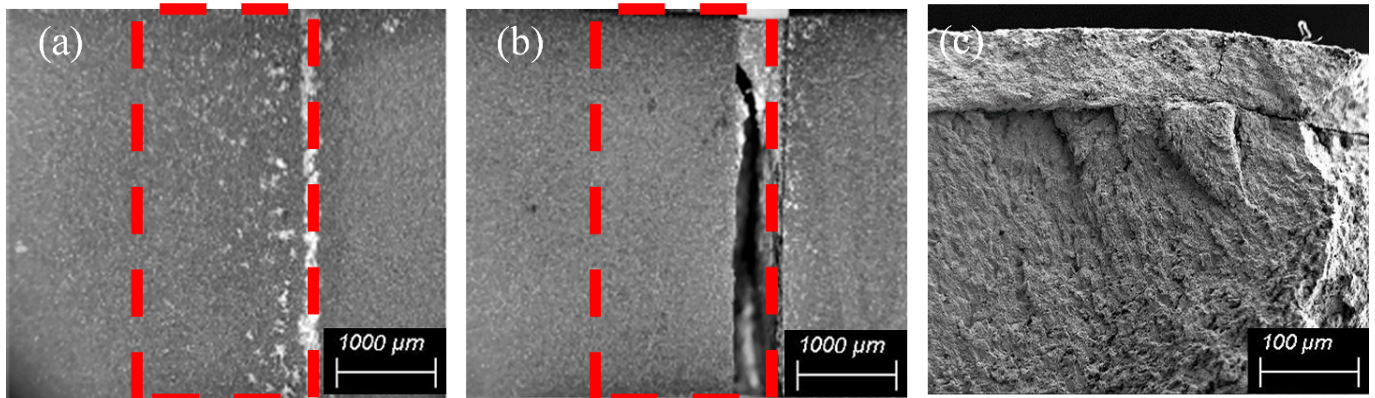


Fig. 11. (a) Contact surface morphology; (b) fretting fatigue fracture position of WC-12Co coated specimen; (c) fretting fatigue fracture morphology of the specimen

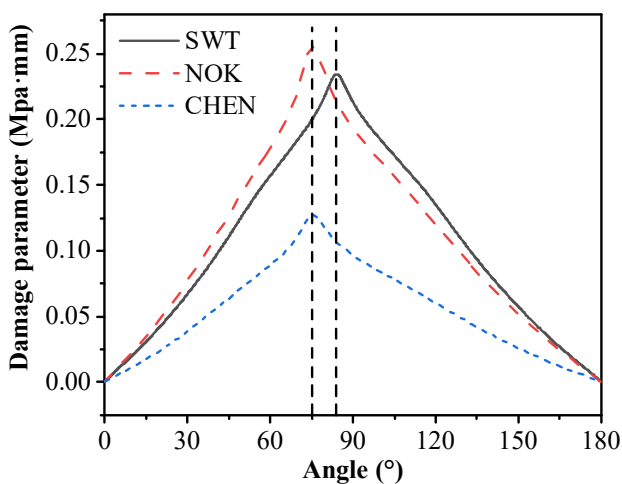


Fig. 12. Damage parameters of WC-12Co coated specimens versus inclination angle  $\theta$

the characteristics of different regions, it can be clearly seen that the fracture can be divided into crack initiation zone, propagation zone and instantaneous break zone. Among them, the crack initiation area is the smallest, which is located on the surface of the coating, which indicates that the crack is initiated on the surface of the specimen.

As shown in Fig. 12, three fatigue damage parameters on different planes are compared when the cyclic axial load is 10 kN. At  $0^\circ$  and  $180^\circ$ , the three fatigue damage parameters have the smallest values, and the largest values appear between  $75^\circ$  to  $90^\circ$ . Among them, SWT parameter is the largest at  $84^\circ$ , NOK parameter and CHEN parameter are all the largest at  $75^\circ$ . The damage parameter values and initiation directions predicted by the three fretting fatigue models under different cyclic loads  $F$  are shown in TABLE 4. It can be seen that the change of crack initiation angle predicted by the three models is very small under

TABLE 4

The values of the fretting fatigue damage parameters and inclination angles under different cyclic load  $F$

Load/kN	CHEN		NOK		SWT	
	Values	Angles	Values	Angles	Values	Angles
8.000	0.09258	77.00°	0.1852	77.00°	0.1633	86.00°
8.500	0.1038	77.00°	0.2075	77.00°	0.1833	86.00°
9.000	0.1146	76.00°	0.2293	76.00°	0.2030	85.00°
9.500	0.1278	76.00°	0.2555	76.00°	0.2178	85.00°
10.00	0.1380	75.00°	0.2760	75.00°	0.2478	84.00°

different cyclic axial loads. The CHEN and NOK parameters obtained similar results. The predicted initiation angle of the CHEN and NOK parameter is between 75° to 77°, while the predicted angle of the SWT parameter is between 84° to 86°. The crack initiation angle obtained in the experiment is shown in Fig. 13. It can be seen that the crack initiation angle is approximately 84° to 86°, which is consistent with the prediction results of SWT parameters. The SWT parameter has more accurate results than the other two parameters in predicting the fretting fatigue crack initiation angle of WC coatings [10,11,19,20]. It can be seen that SWT damage parameter is more suitable for fretting fatigue prediction of WC-12Co coating than NOK and CHEN damage parameters. Therefore, the SWT damage criterion is used in the following discussion. By changing the cyclic load  $F$ , the normal load  $P$  and the friction coefficient  $f$ , the effects of these factors on the fretting damage parameters is investigated.

#### 4.2. Effect of fretting parameters on Smith-Watson-Topper damage factors

Let the normal load  $P = 130$  MPa, and the friction coefficient  $f = 0.5$ , the results of the SWT fatigue damage parameters under cyclic load  $F = 8$  kN, 8.5 kN, 9 kN, 9.5 kN and 10 kN, are shown in Fig. 14(a). It can be seen that the SWT fatigue damage parameter first decreases and then increases along the positive  $x$ -axis, and the minimum value appears at  $x = 5.25$  mm. The change speed at the inner edge and the outer edge is more obvious than the middle part. It can be inferred that the stress increases due to the stress concentration at the contact edge, which leads to the increase of the SWT fatigue damage parameter. With the uniform increase of the applied cyclic load  $F$ , the peak value of the SWT fatigue damage parameter gradually increases, while being closer to the inner edge of the contact pad.

Let the cyclic load  $F = 9$  kN and friction coefficient  $f = 0.5$ , the results of the SWT fatigue damage parameters under the normal load  $P = 110$  MPa, 120 MPa, 130 MPa, 140 MPa and 150 MPa are shown in Fig. 14(b). It can be seen that the SWT fatigue damage parameter shows a trend of first decreasing and then increasing with the increase of the coordinate  $x$ . The SWT fatigue damage parameters near the inner and outer edges increase with the increase of normal load  $P$ , while in the middle part, the SWT fatigue damage parameters decrease with the increase of normal load. Similarly, the position of the minimum value of the SWT fatigue damage parameter also moves along the  $x$ -axis as the normal load  $P$  increases. Similarly, the minimum

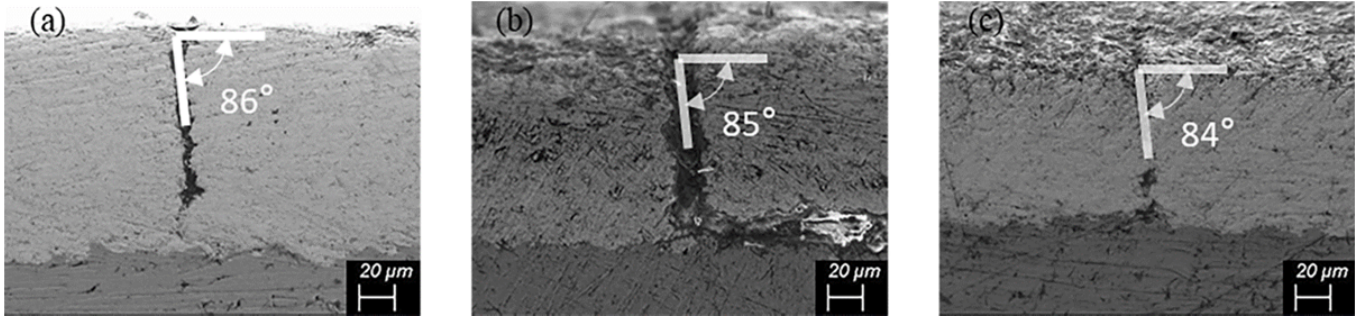


Fig. 13. Cracking angles of cyclic load in different axial direction: (a) 8 kN, (b) 9 kN, (c) 10 kN

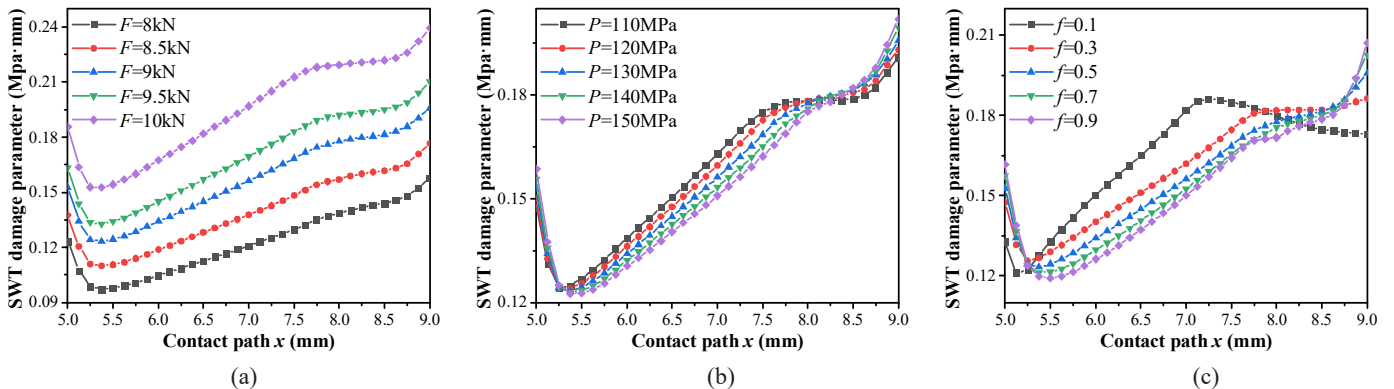


Fig. 14. Variation of SWT damage parameters versus  $x$  coordinate corresponding to different (a) cyclic loading  $F$ , (b) normal loading  $P$  and (c) friction coefficient  $f$

location of SWT fatigue damage parameters also moves along the  $x$ -axis with the increase of normal load  $P$ .

Let the cyclic load  $F = 9$  kN, normal load  $P = 110$  MPa, the results of the SWT fatigue damage parameters corresponding to friction coefficient  $f = 0.1, 0.3, 0.5, 0.7$  and  $0.9$  are shown in Fig. 14(c). It can be seen that the friction coefficient  $f$  has a great influence on the SWT fatigue damage parameters along the contact path  $x$ . The SWT fatigue damage parameters show a trend of first decreasing and then increasing with the increase of coordinate  $x$ , and the location of the minimum value also moves with the increase of friction coefficient  $f$ . However, as the friction coefficient  $f$  decreases, the SWT fatigue damage parameters in the middle of the contact area gradually increases, and when the friction coefficient  $f = 0.1$ , the SWT fatigue damage parameters at  $x = 7.25$  mm exceeds those at the outer edge. This is because when the normal load  $P$  is constant, as the friction coefficient  $f$  decreases, the slip area gradually increases, and the area where the normal load  $P$  acts decreases. The SWT fatigue damage parameter at the middle of the contact area is larger than the value at the outer edge of the contact surface.

## 5. Conclusions

In this paper, by means of fretting fatigue experiment and finite element analysis of tungsten carbide coated specimens, and using the critical plane method, three strain energy density criteria are established to judge the location and direction of fretting fatigue crack initiation and predict fretting fatigue life. The main conclusions are as follows:

- (1) The predicted locations of crack initiation predicted by the Smith-Watson-Topper, Nita-Ogata-Kuwabara and Chen parameters are similar. Although the absolute amplitudes of each parameter are different, it does not affect the judgment of crack initiation location.
- (2) For the prediction of the cracking angle, the predicted results of Smith-Watson-Topper damage parameters are in complete agreement with the experimental results, which indicates that this parameter is more suitable for judging the crack initiation orientation than Nita-Ogata-Kuwabara and Chen parameters.
- (3) The axial cyclic load  $F$  has little effect on the crack location, but the Smith-Watson-Topper damage parameters decreases with the increase of the cyclic load; An increase in the normal load  $P$  make the Smith-Watson-Topper damage parameters more concentrated at the outer edge of the contact surface; A reducing in the friction coefficient  $f$  will increase the Smith-Watson-Topper damage parameters in the middle area of the contact surface.

## Acknowledgments

The authors acknowledge the support of National Natural Science Foundation of China under grant No. 51975411, the Natural Science

Foundation of Tianjin, China under grant No. 18JCYBJC88500, and the Tianjin Postgraduate Scientific Research Innovation Project under grant No. 2020YJSB072.

## REFERENCE

- [1] R.J.K. Wood, Tribology of thermal sprayed WC-Co coatings, Int. J. Refract. Metals Hard Mater. **28** (1), 82-94 (2010). DOI: <https://doi.org/10.1016/j.jrmhm.2009.07.011>
- [2] G. Bolelli, L.M. Berger, M. Bonetti, L. Lusvarghi, Comparative study of the dry sliding wear behaviour of HVOF-sprayed WC-(W, Cr)2C-Ni and WC-CoCr hardmetal coatings, Wear. **309** (1-2), 96-111 (2014). DOI: <https://doi.org/10.1016/j.wear.2013.11.001>
- [3] N. Ma, L. Guo, Z. Cheng, H. Wu, F. Ye, K. Zhang, Improvement on mechanical properties and wear resistance of HVOF sprayed WC-12Co coatings by optimizing feedstock structure, Appl. Surf. Sci. **320**, 364-371 (2014). DOI: <https://doi.org/10.1016/j.apsusc.2014.09.081>
- [4] K. Kubiak, S. Fouvry, A.M. Marechal, J.M. Vernet, Behaviour of shot peening combined with WC-Co HVOF coating under complex fretting wear and fretting fatigue loading conditions, Surf. and Coat. Tech. **201** (7), 4323-4328 (2006). DOI: <https://doi.org/10.1016/j.surfcoat.2006.08.094>
- [5] L. Benea, S.B. Başa, E. Dănăilă, N. Caron, O. Raquet, P. Ponthiaux, Fretting and wear behaviors of Ni/nano-WC composite coatings in dry and wet conditions, Mater. and Des. **65**, 550-558 (2015). DOI: <https://doi.org/10.1016/j.matdes.2014.09.050>
- [6] H.W. Liu, X.J. Xu, M.H. Zhu, P.D. Ren, Z.R. Zhou, High temperature fretting wear behavior of WC-25Co coatings prepared by D-gun spraying on Ti-Al-Zr titanium alloy, Tribol. Int. **44** (11), 1461-1470 (2011). DOI: <https://doi.org/10.1016/j.triboint.2011.01.002>
- [7] J. Luo, Z. Cai, J. Mo, J. Peng, M. Zhu, Friction and wear properties of high-velocity oxygen fuel sprayed WC-17Co coating under rotational fretting conditions, Chinese J. of Mech. Eng. **29** (3), 515-521 (2016). DOI: 10.3901/CJME.2016.0307.026
- [8] J.H. Lee, I.H. Oh, J.H. Jang, S.K. Hong, H.K. Park, Mechanical properties and microstructural evolution of WC-binderless and WC-Co hard materials by the heat treatment process, J. of Alloys and Compd. **786**, 1-10 (2019). DOI: <https://doi.org/10.1016/j.jallcom.2019.01.282>
- [9] C. Hu, D. Wei, Y. Wang, L. Shi, Experimental and numerical study of fretting fatigue in dovetail assembly using a total life prediction model, Eng. Fract. Mech. **205**, 301-318 (2019). DOI: <https://doi.org/10.1016/j.engfracmech.2018.08.001>
- [10] J. Vázquez, C. Navarro, J. Domínguez, Analysis of fretting fatigue initial crack path in Al7075-T651 using cylindrical contact, Tribol. Int. **108**, 87-94 (2017). DOI: <https://doi.org/10.1016/j.triboint.2016.09.023>
- [11] A. Nitta, A. Ogata, K. Kuwabara, Fracture mechanisms and life assessment under high-strain biaxial cyclic loading of type 304 stainless, Fatigue Fract. Eng. Mater. Struct. **12** (2), 77-92 (1989). DOI: <https://doi.org/10.1111/j.1460-2695.1989.tb00515.x>

- [12] X. Chen, S. Xu, D. Huang, A critical plane-strain energy density criterion for multiaxial low-cycle fatigue life and under non-proportional loading, *Fatigue Fract. Eng. Mater. Struct.* **22** (8), 679-686 (1999).  
DOI: <https://doi.org/10.1046/j.1460-2695.1999.t01-1-00199.x>
- [13] Richard C. Rice, *Fatigue Design Handbook*, England 1988.
- [14] M.G. Yan, *China aeronautical materials handbook*, China 2001.
- [15] L. Xu, H. Jing, L. Huo, Young's modulus and stress intensity factor determination of high velocity electric arc sprayed metal-based ceramic coatings, *Surf. and Coat. Tech.* **201** (6), 2399-2406 (2006).  
DOI: <https://doi.org/10.1016/j.surfcoat.2006.04.021>
- [16] Y. Mutoh, T. Hattori, K. Nagata, Fretting fatigue test method for JSME standard, *The Proceedings of JSME Annual Meeting* **1**, 453-454 (2002).
- [17] Z. Zhuang, F. Zhang, S. Cen, *The nonlinear FEM analysis and examples of ABAQUS*, Beijing 2005.
- [18] R. Gutkin, B. Alfredsson, Growth of fretting fatigue cracks in a shrink-fitted joint subjected to rotating bending, *Eng. Fail. Anal.* **15**, 582-596 (2008).  
DOI: <https://doi.org/10.1016/j.engfailanal.2007.04.003>
- [19] C. Navarro, J. Vázquez, J. Domínguez, Nucleation and early crack path in fretting fatigue, *Int. J. Fatigue* **100**, 602-610 (2008).  
DOI: <https://doi.org/10.1016/j.engfailanal.2007.04.003>
- [20] J. A. Araújo, G.M.J. Almeida, J.L.A. Ferreira, C.R.M. da Silva, F.C. Castro, Early cracking orientation under high stress gradients: the fretting case, *Int. J. Fatigue* **100**, 611-618 (2017).  
DOI: <https://doi.org/10.1016/j.engfailanal.2007.04.003>